Chemical Engineering Journal Advances 25 (2026) 101011

Contents lists available at ScienceDirect

Chemical Engineering Journal Advances

journal homepage: www.sciencedirect.com/journal/chemical-engineering-journal-advances

Sustainable removal of methylene blue using minimally modified hydrochar from durian peels with experimental adsorption and density functional theory studies

Piangjai Peerakiatkhajohn [a], Praewa Wongburi [a], Kamonwat Nakason [b], Bunyarit Panyapinyopol [b], Khanin Nueangnoraj [c], Phongphot Sakulaue [d], Davide Poggio [e], William Nimmo [f], Jakkapon Phanthuwongpakdee [a,*]

[a] Faculty of Environment and Natural Resource Studies, Mahidol University, Nakhon Pathom 73170, Thailand
[b] Department of Sanitary Engineering, Faculty of Public Health, Mahidol University, Bangkok 10400, Thailand
[c] School of Bio-Chemical Engineering and Technology, Sirindhorn International Institute of Technology, Thammasat University, Pathum Thani 12120, Thailand
[d] Division of Chemical Engineering, Faculty of Engineering, Rajamangala University of Technology Krungthep, Bangkok 10120, Thailand
[e] School of Chemical, Materials and Biological Engineering, Faculty of Engineering, University of Sheffield, Sheffield S10 2TN, United Kingdom
[f] School of Mechanical, Aerospace and Civil Engineering, University of Sheffield, Sheffield S10 2TN, United Kingdom

ARTICLE INFO

Keywords:
Durian peels
Methylene blue
Hydrochar
Hydrothermal carbonization
Adsorption
Density functional theory

ABSTRACT

This study investigated the use of hydrochar (HC) derived from durian peels as an adsorbent for removing methylene blue (MB) from an aqueous environment. HC was synthesized from durian peels using hydrothermal carbonization under varying temperature (160 – 200 °C) and time (2 – 6 h) conditions. The optimal condition 180 °C for 2 h (HC-180–2) was identified. HC-180–2 was evaluated in MB adsorption experiments and adsorbent characterization. It achieved a maximum MB adsorption capacity (q) of 51.6 mg/g at room temperature, reaching equilibrium within 150 min, and the q value increased to 59.2 mg/g at 65 °C. The adsorption followed pseudo-second-order kinetics ($R^2 = 0.996$) and Langmuir isothermal behavior ($R^2 = 0.996$), indicating chemisorption on energetically uniform adsorption sites. Thermodynamic analysis yielded Gibbs free energy values ranging from -43.0 to -55.3 kJ/mol and an enthalpy change of 48.5 kJ/mol, which further confirmed the spontaneous and endothermic nature of the chemisorption process. The surface area of HC-180–2 increased from 3.04 to 6.36 m^2/g compared to the biomass, confirming the chemisorption and dependence on chemical functionality rather than physical surface area. Structural characterizations revealed enhanced aromatization and functional group formation, including sulfone and ester groups. Density functional theory calculations revealed two possible HC-MB conformation with adsorption mechanisms involving hydrogen bonding, π-π stacking and π-sulfur interactions. The chemisorption nature was also confirmed through Quantum Theory of Atoms in Molecules electron density pathway analysis. While the adsorption capacity was moderate compared to chemically modified adsorbents, the minimally processed durian peels HC positioned itself as a promising green alternative for MB removal.

1. Introduction

Among many organic dyes, methylene blue (MB) has diverse applications across the pharmaceutical, paper, paint, medical, and food industries [1]. It is particularly prevalent in the textile industry, where it is widely recognized as one of the most commonly used colorants for fabrics [1]. The textile industry alone contributes over half of the global dye effluent, accounting for 55 % of the total [2]. Long-term animal studies have indicated that MB is carcinogenic and poses a serious threat to human health [3]. Its aromatic ring structure confers high chemical stability and poor biodegradability, enabling persistence and wide dispersion once released; untreated or insufficiently treated industrial and medical effluents are the principal pathways by which MB enters aquatic systems [4]. No research has monitored actual MB quantity, but a study claimed 10 – 200 mg/L to be the concentration range of MB found in the wastewater effluent from various textile processes [5]. Another study employed actual dyeing industrial effluent in the adsorption study, in which the concentration of MB could reach 1000

* Corresponding author.
E-mail address: jakkapon.pha@mahidol.ac.th (J. Phanthuwongpakdee).

https://doi.org/10.1016/j.ceja.2025.101011

Available online 23 December 2025

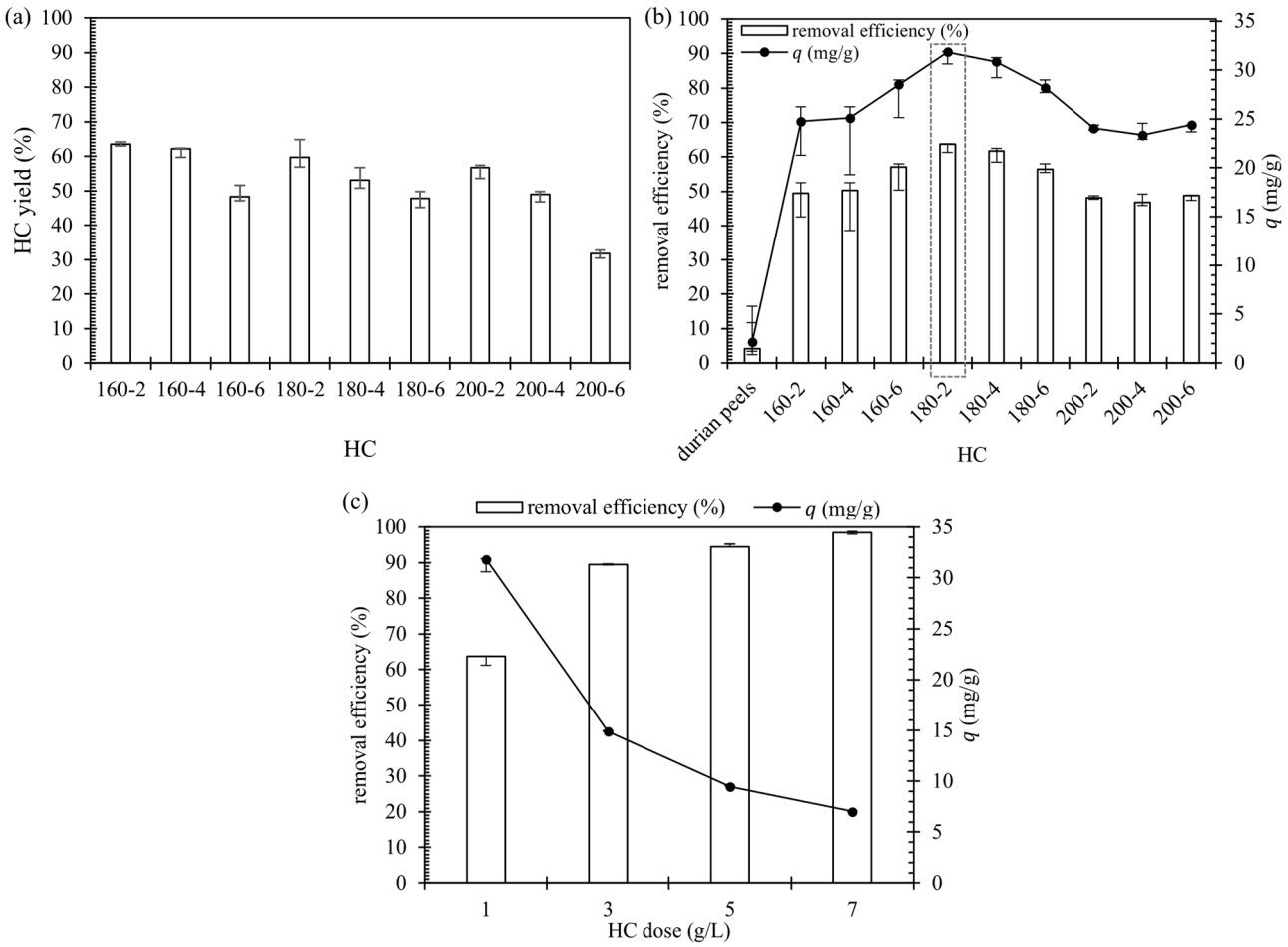

Fig. 1. HC yield and removal efficiency at different hydrothermal treatment conditions: (a) HC yields at 160, 180, and 200 °C for 2, 4 and 6 h (Eq. (1)), (b) MB removal efficiency with durian peels and HC produced at 160, 180, and 200 °C for 2, 4 and 6 h, (c) HC-180–2 of doses 1, 3, 5, and 7 g/L for 30 min. Adsorption experiments were performed with an initial MB concentration of 50 mg/L at room temperature.

mg/L [6]. Untreated or insufficiently treated industrial and medical effluents are the primary pathways by which MB enters the aquatic systems, with its water solubility and environmental stability enabling it to spread widely and persist. Effective natural and engineered remediation processes are essential for mitigating their environmental impact [7,8].

Various methods have been developed for dye removal, including biological treatment [9,10], membrane separation [11,12], coagulation [13,14], photocatalytic processes [15,16], and adsorption techniques [17–19]. Conventional wastewater treatment methods often achieve only partial removal of MB, with performance sensitive to influent concentration and matrix complexity, leaving residual contamination risks [20]. Phytoremediation using wetland plants is a promising green technology for reducing MB in aquatic environments, especially as a tertiary step after primary wastewater treatment [8]. However, phytoremediation is slow and carries a risk of secondary pollution if not properly managed. Its success greatly depends on specific plant types and environmental conditions. Photocatalytic degradation is another method for MB mineralization, facilitated by the generation of reactive species that promote oxidation–reduction activity under light illumination. However, many efficient systems rely on metal-based catalysts (e.g. Fe, Ce, Ti), and high catalyst loadings may pose additional environmental concerns [21–23]. Hence, the adsorption process is favorable due to its rapid kinetics, high efficiency, operational simplicity, and ability to operate independently of sunlight or biological growth cycles.

Carbonaceous adsorbents are often used for MB adsorption. Pyrolysis-derived biochar and activated carbons perform well but typically require high temperatures during the production process (400 – 700 °C), which drives energy demand for both heating and biomass drying [24,25]. Hydrothermal carbonization (HTC) provides a lower-temperature, water-mediated route (about 180 – 250 °C) that converts wet biomass directly into hydrochar (HC) similar to the geological formations of a sealed aqueous system, avoiding the energy penalty of prior drying [26]. Previous work has demonstrated MB adsorption by HC from various fruit peels, with maximum capacities of around 21 mg/g [27]. In contrast, chemically modified HC samples often perform substantially better. For example, the activation of sugarcane bagasse HC with phosphoric acid and NaOH yielded capacities of up to 357 mg/g [28], and the addition of poly(vinyl chloride) during the HTC of bamboo powder produced HC that adsorbed 259 mg/g MB [28]. However, these modification routes introduced additional chemical inputs during synthesis, which undermine the fundamental criteria of sustainability and environmental compatibility required for green adsorbents.

Durian (*Durio zibethinus*), a popular seasonal fruit in tropical countries, is renowned for its distinctive flavor and unique aroma. Thailand is the leading producer of durian (production volume of about 1.68 million tons as of March 2025), with other countries like Vietnam, Malaysia, Indonesia, and the Philippines also contributing [29,30]. Only about 20 – 30 % of the fruit is edible, while the remaining 70 – 80 %, which consists of the durian peels (also known as durian shell), is typically discarded as waste [29]. At 2025 production levels, this implies approximately 1.34 million tons of peel waste annually in Thailand alone. The waste biomass has been widely utilized as fertilizer, animal

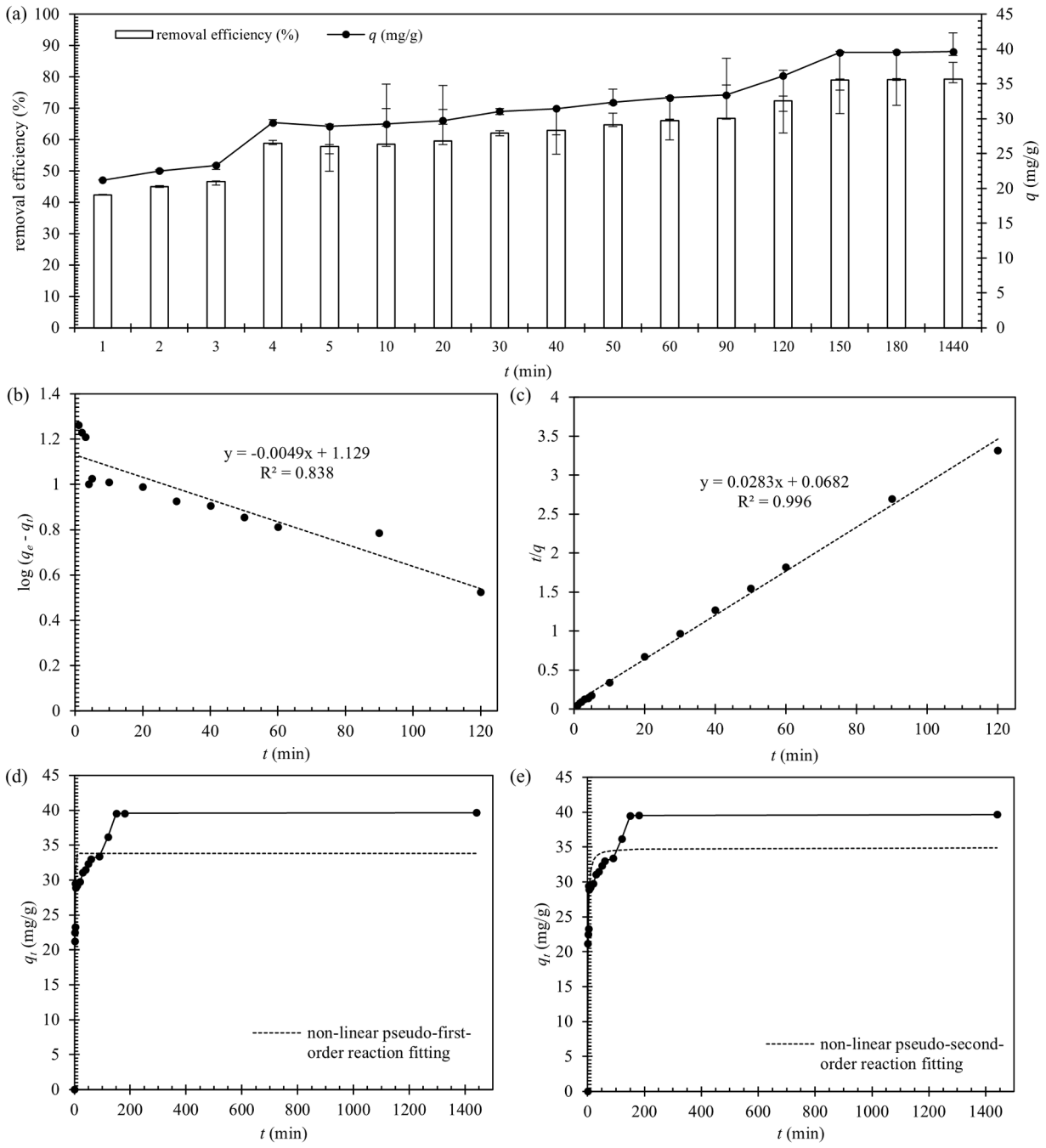

Fig. 2. Kinetic experiments and fittings of pseudo-order reaction models: (a) MB removal efficiency by HC-180–2 at different contact times (1 – 1440 min), (b) linear pseudo-first-order reaction (Eq. (4)), (c) linear pseudo-second-order reaction (Eq. (5)), (d) non-linear pseudo-first-order reaction (Eq. (6)), (e) non-linear pseudo-second-order reaction (Eq. (7)). Kinetic experiments were performed with an HC optimal dose and an initial MB concentration of 50 mg/L at room temperature.

Table 1
Parameters for linear and non-linear pseudo-order reaction models. Kinetic experiments were conducted at various contact times (1 – 1440 min) with an HC optimal dose and an initial MB concentration of 50 mg/L at room temperature.

pseudo-first-order reaction						pseudo-second-order reaction					
linear[a]			non-linear[b]			linear[c]			non-linear[d]		
k_1 (L/min)	q_e (mg/g)	R^2	k_1 (L/min)	q_e (mg/g)	R^2	k_2 (L/min)	q_e (mg/g)	R^2	k_2 (L/min)	q_e (mg/g)	R^2
−0.0113	13.5	0.838	0.560	33.8	0.855	0.0113	30.5	0.996	0.069	34.9	0.913

a. values calculated from Eq. (4).
b. values calculated from Eq. (5).
c. values calculated from Eq. (6).
d. values calculated from Eq. (7).

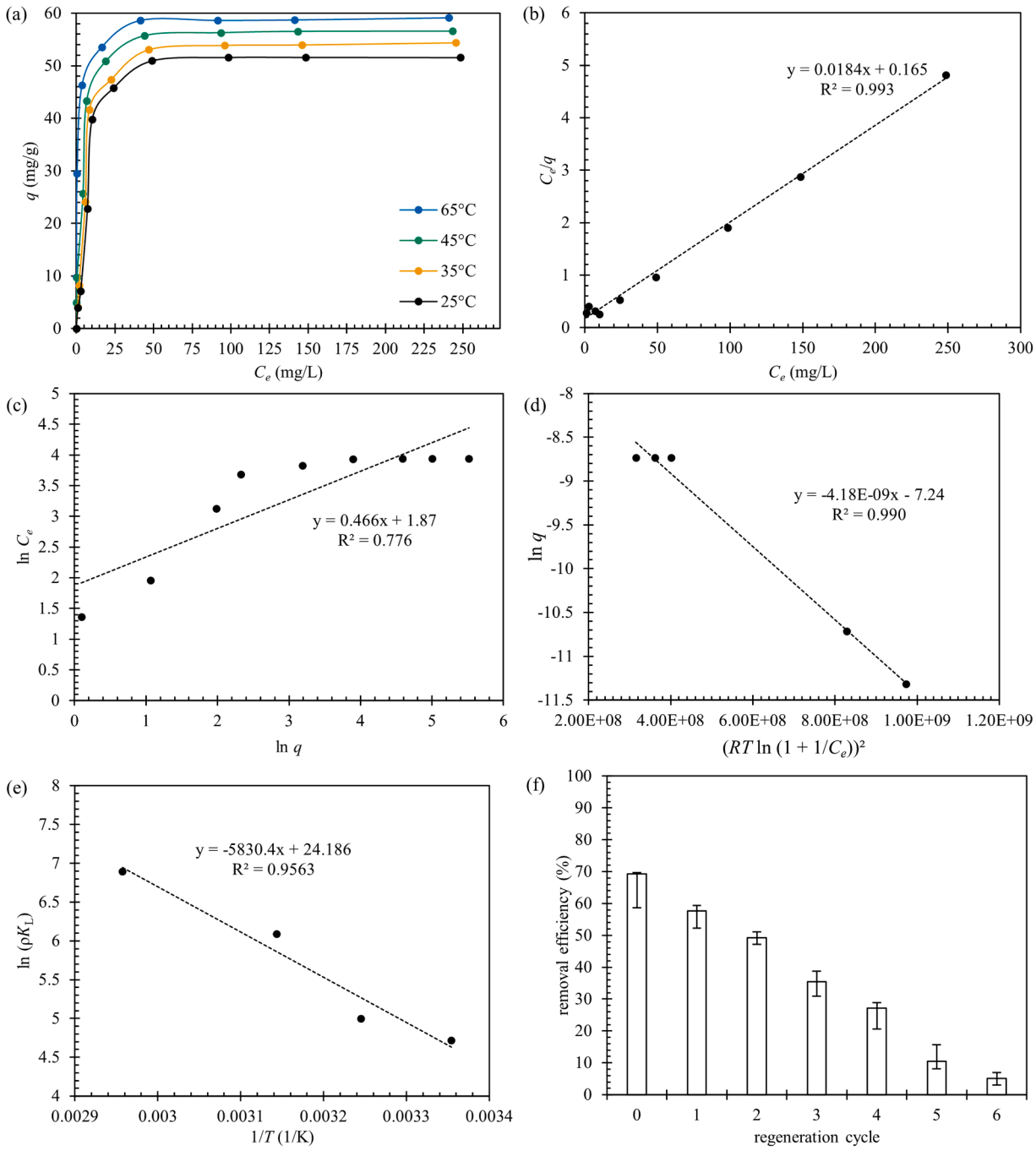

Fig. 3. Isothermal fittings and reusability of HC: (a) MB adsorption capacity (q, mg/g) against different MB final concentration (C_e, mg/L) at various temperatures, (b) fitting of the Langmuir model (Eq. (8)), (c) fitting of the Freundlich model (Eq. (9)), (d) fitting of the D-R model (Eq. (10)), (e) fitting of the Van 't Hoff equation (Eq. (12)), (f) reusability of HC-180–2 for MB adsorption over 6 consecutive regeneration cycles using 50 mg/L MB solution. Adsorption data at initial MB concentrations ranging from 0 to 300 mg/L and at room temperature were used to fit isothermal model. Isotherm and thermodynamic experiments were conducted using the optimal adsorbent dosage and contact time.

Table 2
Parameters for Langmuir and Freundlich models. Initial MB concentrations of 0 – 300 mg/L were used at room temperature, optimal adsorbent dosage and contact time.

Langmuir isotherm [a]			Freundlich isotherm [b]			*D-R isotherm* [c]			
q_{max} (mg/g)	K_L (L/mg)	R^2	n	K_F ($mg^{1-1/n}L^{1/n}/g$)	R^2	q_{max} (mg/g)	$K_{D\text{-}R}$ (mol^2/J^2)	$E_{D\text{-}R}$ (kJ/mol)	R^2
54.3	0.112	0.996	2.15	6.48	0.916	61.9	1.56×10^8	5.66	0.971

a. values calculated from Eq. (8).
b. values calculated from Eq. (9).
c. values calculated from Eqs. (10) and (11).

Table 3
Parameters for thermodynamic calculations. Initial MB concentrations of 0 – 300 mg/L were used at room temperature, optimal adsorbent dosage and contact time.

Thermodynamic parameters				
T (°C)	K_L (L/mg) [a]	ΔH (kJ/mol) [b]	ΔS (kJ/K/mol) [b]	ΔG (kJ/mol) [c]
25	0.112	48.5	0.307	−43.0
35	0.148			−46.1
45	0.441			−49.1
65	0.988			−55.3

a. values calculated from Eq. (8) (linear fit of Langmuir isotherm model of all temperature conditions can be found in Fig. S2).
b. values calculated from Eq. (12).
c. values calculated from Eq. (13).

Table 4
Surface properties of durian peels and HC-180–2 determined from nitrogen adsorption-desorption isotherms.

sample	BET [a]			BJH (adsorption branch) [b]	
	surface area (m^2/g)	total pore volume (cm^3/g)	C[c]	average pore diameter (nm)	total pore volume (cm^3/g)
durian peels	3.04	0.698	6.98	16.0	0.0347
HC-180–2	6.36	1.46	24.2	29.9	0.0430

a. Brunauer–Emmett–Teller method.
b. Barrett–Joyner–Halenda method.
c. BET C constant, indicating the strength of adsorption.

Table 5
Elemental composition (wt. %) of durian peels and HC-180–2 before and after MB adsorption, determined by EDX.

sample	elemental composition (wt. %)				
	carbon (C)	oxygen (O)	sulfur (S)	magnesium (Mg)	potassium (K)
durian peels	52.5	45.8	0.100	0.330	1.30
HC-180–2	58.3	41.6	0.100	-	-
HC-180–2 (after MB adsorption)	57.6	42.2	0.220	-	-

feed, catalysts, and bio-energy production [29,31–33]. However, given the large quantities generated, exploring its use as a water pollutant adsorbent offers significant potential for broader valorization. This is especially true for the adsorption of MB. Prior studies have reported effective MB removal using activated carbon derived from durian shells, with capacities up to 96.7 mg/g [34–36].

Computational chemistry based on density functional theory (DFT) is widely used to investigate the interactions between MB and carbon-based adsorbents. For instance, the Becke exchange functional with the Lee-Yang-Parr correlation functional (BLYP) with the 6–31++G(d,p) basis set was employed to examine the interactions between MB and NaOH-activated biochar derived from *Aurantii Fructus Immaturus* at 800 °C [37]. The study indicated that the adsorption process was governed by interactions between the -OH, -COOH, and -NH—CO- functional groups of the adsorbent and the amino groups of MB [37]. The generalized gradient approximation and BLYP were also employed to investigate the interactions between NaOH-activated pyrolyzed biochar and MB, revealing that the strongest interaction occurs between the –COOH groups of the adsorbent and the R–N(CH_3)$_2$ groups of MB. Another study employed DFT-D3 with the 6–311+G basis set to inspect MB adsorption onto HC activated with potassium citrate and iron citrate, and it revealed that the mechanism was driven by π–π interactions, electrostatic forces, and hydrogen bonding [38]. Molecular dynamics simulation was also used to study the adsorption of MB onto green peel material, and it calculated the spontaneous reaction with an adsorption energy of −75.8 kcal/mol [39]. Nevertheless, realistic adsorption simulations should include initial molecular docking to identify energetically favorable binding configurations before conducting geometry optimization. Additionally, Quantum Theory of Atoms in Molecules (QTAIM) analysis remains essential for quantitatively assessing bond critical points and electron density topology, thereby differentiating between physisorption and chemisorption mechanisms.

As a lower-energy alternative, HC from HTC from wet biomass under moderate conditions, without prior drying, offers a promising pathway. To date, MB adsorption using minimally modified HC from durian peels has not been systematically evaluated, and no computational studies using docking and QTAIM have yet elucidated the associated adsorption mechanisms. It is hypothesized that minimally processed HC from durian peels can effectively remove MB through mechanisms involving functional group interactions.

This study aims to synthesize HC from durian peels via low-temperature HTC and comprehensively evaluate its MB adsorption performance in water. Durian peels HC was successfully produced via HTC at temperatures below 200 °C under inert conditions. Adsorption kinetics, isotherms, and thermodynamics were analyzed to understand the adsorption behavior and capacity, while computational chemistry methods provided molecular-level insights into the interactions between HC-MB. Collectively, the results offer a comprehensive evaluation of minimally processed durian peels HC as an effective and eco-friendly adsorbent for removing MB.

2. Methodology

2.1. Hydrochar preparation

Durian (*Durio zibethinus* Murray) peels were obtained from a local market. The biomass was thoroughly washed with tap water to remove excess dirt, then rewashed with DI water. The clean biomass was oven-dried at 70 °C for 24 h or until its weight remained constant. Then, it was ground using a grinder before being sieved with standard aluminium sieves to obtain the sample with sizes smaller than 125 μm.

The prepared durian peels (3 g) were mixed with 30 mL of deionized water (biomass-to-water ratio of 1:10 w/v) and placed in a 100 mL hydrothermal reactor with a Teflon chamber, followed by heating in a hot-air oven at 160, 180, and 200 °C for residence times of 120, 240, and 360 min. The reactor was sealed and allowed to reach the target temperature naturally within the oven, with no external pressure control (autogenous pressure). After the residence time, the reactor was immediately placed in cool water to stop further reaction. The resulting products were then filtered through Whatman™ No. 4 filter paper, and the recovered HC was subsequently dried at 70 °C for 24 h or until a constant weight was achieved. The yield of HC was calculated using Eq. (1), based on the mass of HC produced (g) and the mass of its precursor, dry durian peels (g).

$$HCyield(\%) = (mass of HC \,/\, mass of dry durian peels) \times 100 \quad (1)$$

2.2. Adsorption experiments

MB (QReC™, New Zealand) was used as obtained. The adsorption efficiency of MB by HC was evaluated by first preparing a calibration. Standard MB solutions with concentrations of 20, 40, 60, 80, 100, and 300 mg/L were measured at 667 nm using a UV–Visible spectrophotometer. The resulting calibration plot is presented in the supplementary material (Fig. S1). At the end of every adsorption experiment, the mixture of HC and solute was gently shaken and left to stand at room temperature for 120 min. Afterwards, it was centrifuged at 4400 rpm for

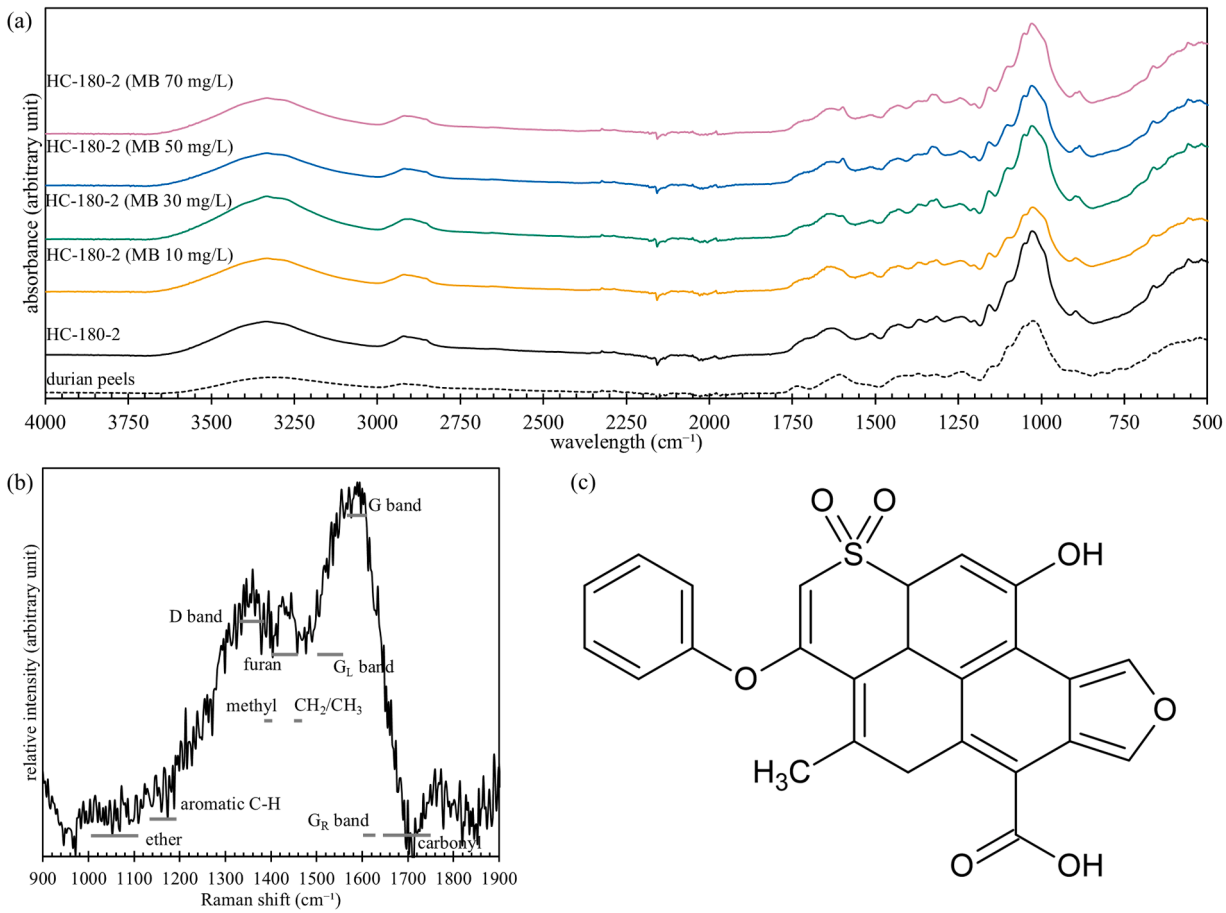

Fig. 4. Chemical functional groups and proposed structures of HC: (a) FTIR absorbance spectrum of durian peels and HC-180–2, before and after MB adsorption, (b) Raman shifts of HC-180–2, adopted from a previous study [62], (c) proposed HC structure derived from FTIR spectrum and Raman shifts.

30 min. The supernatant was analyzed by UV–Visible spectrophotometry (V-750, Jasco, Japan) at 667 nm, and the absorbance values were compared with the calibration curve to determine the final MB concentration. All adsorption experiments were carried out in triplicate. The MB removal efficiency (%) was then calculated according to Eq. (2). The adsorption capacity (q, mg/g), referring to the amount of MB adsorbed per unit mass of the HC, was calculated using Eq. (3).

$$\text{MB removal efficiency}(\%) = (C_0 - C_e)/C_0 \times 100 \quad (2)$$

$$q = (C_0 - C_e)/m \times V \quad (3)$$

C_0 (mg/L) and C_e (mg/L) refer to initial and remaining MB concentrations, respectively. The mass of HC used in the adsorption experiments is represented by m (g), while V (L) is the volume of solute. All experiments were performed in triplicate, and a fourth trial was performed if significant variation was observed between the initial results.

The screening test was conducted with a 1 g/L HC dosage at a C_0 of 50 mg/L, maintained at room temperature for 30 min. Then the HC with the best HTC condition was selected for the remainder of the adsorption experiment. For dosage selection, HC at 1, 3, 5, and 7 g/L were used to adsorb 50 mg/L MB at room temperature for 30 min.

To determine the optimal time, adsorption experiments were conducted with contact times ranging from 0 to 1440 min. The optimal HC dosage was used with an initial MB concentration of 50 mg/L at room temperature. The contact time data were fitted to a linear pseudo-first-order reaction (Eq. (4)) and a pseudo-second-order reaction (Eq. (5)). For comparison, the data were also modeled using non-linear reaction equations. The non-linear forms of the pseudo-first-order and pseudo-second-order models are given by Eqs. (6) and (7), respectively.

$$\log(q_e - q_t) = \log q_e - (k_1/2.303)t \quad (4)$$

$$t/q_t = 1/k_2 {q_e}^2 + t/q_e \quad (5)$$

$$q_t = q_e(1 - \exp(-k_1 t)) \quad (6)$$

$$q_t = k_2 {q_e}^2 t/1 + k_2 q_e t \quad (7)$$

q_t (mg/g) represents q at a given time (t), and q_e (mg/g) denotes q at equilibrium. k_1 and k_2 represent the pseudo-first (L/min) and second-order reaction rate constants (g/mg/min), respectively.

Adsorption experiments with varying initial MB concentrations (0 – 300 mg/L) were conducted under the previously established optimal adsorption time and adsorbent dosage. To gather data for thermodynamic analysis, experiments were performed at four different temperatures (25, 35, 45, and 65 °C) for each initial concentration. The equilibrium data were evaluated using the linearized forms of the Langmuir (Eq. (8)) and the Freundlich (Eq. (9)). The Dubinin-Radushkevich (D-R) isotherm model (Eqs. (10) and (11)) was also employed, following the modified form developed explicitly for liquid-solid adsorption systems as reported in previous literature [40]. Thermodynamic parameters were calculated from the linear plots obtained using Eq. (12) and the values derived from Eq. (13).

$$1/q = 1/q_{max} + 1/K_L C_e q_{max} \quad (8)$$

$$\log q = 1/n(\log C_e) + \log K_F \quad (9)$$

$$\ln q = \ln q_{\max} - K_{D-R}(RT(C_s/C_e)) \quad (10)$$

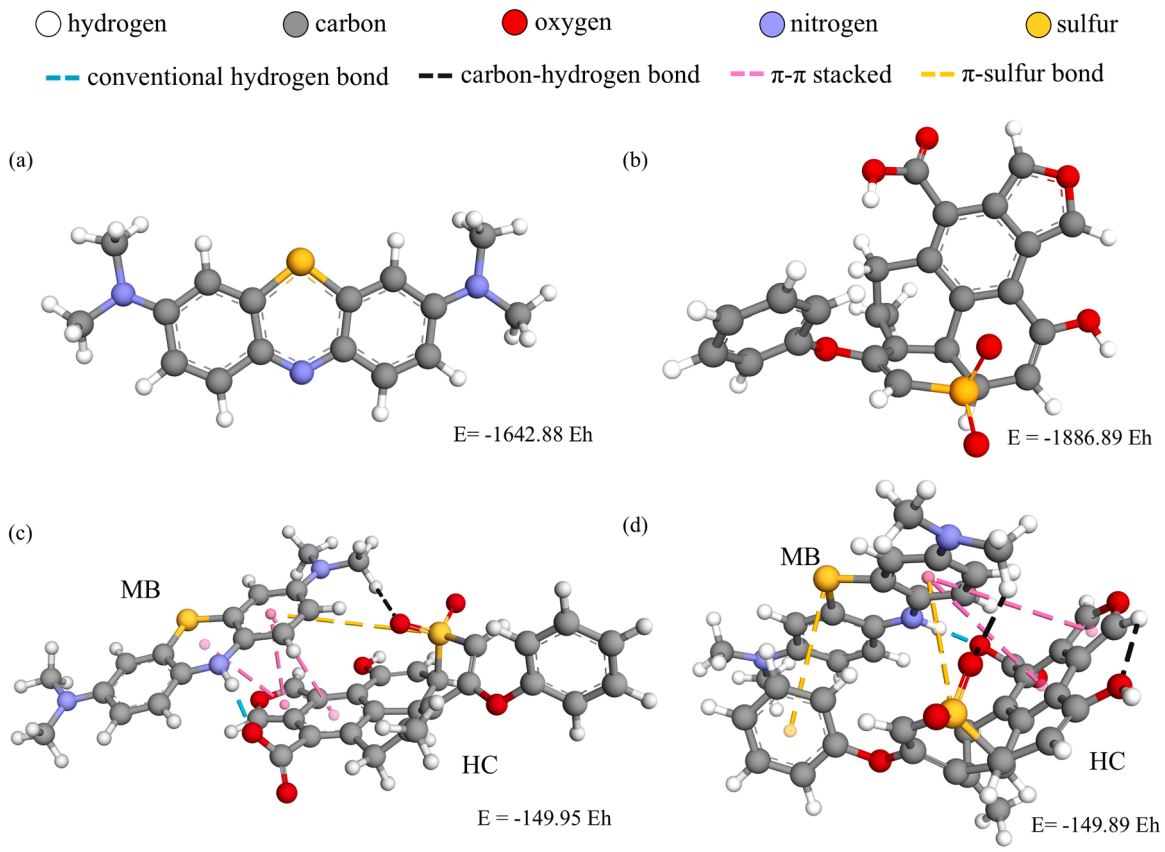

Fig. 5. Optimized structures and HC-MB interactions: (a) optimized MB structure, (b) optimized HC structure, (c) HC-MB conformation with the lowest binding energy (conformation 1), (d) HC-MB conformation with the lowest binding energy (conformation 2).

$$E_{D-R} = 1/\sqrt{(2K)} \tag{11}$$

$$\ln(\rho K_L) = -\Delta H/RT + \Delta S/R \tag{12}$$

$$\Delta G = \Delta H - \Delta TS \tag{13}$$

q_{max} (mg/g) represents the maximum adsorption capacity, indicating the total number of available surface sites on the adsorbent. In the Langmuir isotherm model (Eq. (8)), K_L (L/g) denotes the Langmuir constant. For the Freundlich model (Eq. (9)), K_F ($mg^{1-1/n}L^{1/n}/g$) is the Freundlich constant, and n is the heterogeneity factor, which relates to adsorption intensity and the free energy of adsorption. $K_{D\text{-}R}$ (mol^2/J^2) is associated with the D-R isotherm as the free energy of adsorption per mole of MB, and C_s is the concentration of MB at the saturation point (Eq. (10)). It is used to determine D-R isotherm free energy of the solid-liquid interface ($E_{D\text{-}R}$, kJ/mol), following Eq. (11). Thermodynamic analyses (Eqs. (12) and (13)) were performed using the absolute temperature (T, K) and the universal gas constant (R = 8.314 J/mol/K). ΔH (kJ/mol) is the enthalpy change of adsorption, and ΔS (J/K/mol) is the entropy change, which reflects the degree of randomness at the solid-solution interface during adsorption. The Gibbs free energy change (ΔG, kJ/mol) was determined to evaluate spontaneity. K_L, derived from the Langmuir model, was applied as the distribution coefficient. The Van't Hoff equation (Eq. (12)) was modified to include the water density (ρ, 1000 g/L) to achieve a dimensionless form [41].

The reusability of HC-180–2 was evaluated over 6 consecutive adsorption-regeneration cycles. For each cycle, the optimal adsorbent dosage was used to adsorb MB from a 50 mg/L solution for the equilibrium contact time at room temperature. After each adsorption cycle, the spent HC was separated by filtration and soaked in DI water for 2 h to facilitate desorption of adsorbed MB. The regenerated HC was then dried at 70 °C until it reached a constant weight and subsequently reused in the next adsorption cycle under identical conditions.

2.3. Hydrochar characterization

The HC sample with optimal MB adsorption was used for the characterization. The porous properties of the HC and durian peels were compared and evaluated to identify changes in surface area and porosity caused by HTC. The nitrogen adsorption-desorption measurement was conducted at –195.8 °C (Belsorp MiniX, MicrotracBE Corp., Japan). Brunauer–Emmett–Teller (BET) theory was employed to calculate the specific surface area, and the Barrett, Joyner, and Halenda (BJH) method was used to analyze the pore size distribution. The nitrogen adsorption data at a relative pressure of 0.99 were utilized to determine the total pore volume (V_{total}).

Scanning electron microscopy (SEM, JSM-IT500LA, Japan) was employed to visualize the surface morphology of the durian peels, the derived HC, and the HC after MB adsorption. Additionally, energy-dispersive X-ray spectroscopy (EDX) was employed to analyze the surface elemental composition of these three samples, providing complementary information on the adsorption process.

Fourier-transform infrared spectroscopy (FTIR, Thermo Fisher Scientific, iS50, USA) was carried out on the durian peels, the derived HC, and the HC after MB adsorption to identify and compare the functional groups present. This analysis was used to elucidate the changes in surface chemistry that occur during hydrothermal carbonization and subsequent dye adsorption.

Raman spectroscopy was performed using an atomic force microscope-Raman (OmegaScope, Horiba Scientific, Japan) on the HC to characterize its carbon structure further and provide additional insight into the degree of graphitization and structural disorder. It can also be used to assess some important functional groups.

Table 6
Bond types and functional groups involved in the interactions of HC and MB in conformation 1 and 2.

conformation	bond type	functional groups involved in the interaction		bond length (Å)
		HC	MB	
1 (Fig. 5c)	conventional hydrogen	carboxylic acid (H-donor)	Amine (H-acceptor)	1.81
	carbon-hydrogen bond	Sulfone (H-acceptor)	Methyl (H-donor)	2.64
	π-π stacked	benzene derivative (π orbitals)	benzene derivative (π orbitals)	4.11
		benzene derivative (π orbitals)	benzene derivative (π orbitals)	3.69
		benzene derivative (π orbitals)	benzene derivative (π orbitals)	3.37
	π-sulfur stacked	Sulfone (sulfur)	benzene derivative (π orbitals)	5.81
2 (Fig. 5d)	conventional hydrogen	carboxylic acid (H-donor)	Amine (H-acceptor)	1.74
	carbon-hydrogen bond	Sulfone (H-acceptor)	Methyl (H-donor)	2.46
	π-π stacked	benzene derivative (π orbitals)	benzene derivative (π orbitals)	4.63
		benzene derivative (π orbitals)	benzene derivative (π orbitals)	5.13
	π-sulfur stacked	Sulfone (sulfur)	benzene derivative (π orbitals)	4.42
		benzene derivative (π orbitals)	Thioether (sulfur)	4.58

2.4. Computational studies

The results obtained from FTIR and Raman spectroscopy were used to deduce the HC structure. HC and MB structures were pre-optimized by employing the Becke 1988 and Perdew 1986 (BP86) density functional in combination with the def2-SV(P) basis set. The Resolution of Identity (RI) approximation with NormalSCF convergence criterion was applied to accelerate the computation. Then, the pre-optimized HC structure was further optimized using the semi-empirical GFN2-xTB method, as implemented in the xTB engine. Solvent effects were modeled with the ALPB(Water) implicit solvation approach. The calculation was executed in a %DOCKER environment with the pre-optimized MB structure as a guest molecule. A more computationally expensive method, utilizing the Becke, 3-parameter, Lee–Yang–Parr (B3LYP) hybrid functional with the def2-TZVP basis set and a TightSCF convergence criterion, was employed to calculate the single-point energy for the final HC-MB structure. The computational analysis was conducted using ORCA 6 with the SHARK integral generation and digestion engine [42,43]. QTAIM analysis was performed with Multiwfn 3.8 [44]. All molecular visualizations will be generated using Chemcraft 1.8 and Discovery Studio 2025 [45,46].

3. Results and discussion

3.1. Adsorption of methylene blue by hydrochar

Durian peel-derived HC samples were successfully produced under varying hydrothermal conditions. Fig. 1a presents the HC yields obtained from durian peel biomass under various hydrothermal carbonization conditions. The nomenclature used (e.g., 160–2, 180–4, 200–6) denoted the reaction temperature (°C) and residence time (h), respectively. The results demonstrated that HC yield was inversely correlated with both temperature and residence time. The increase in carbonization temperature from 160 °C to 200 °C progressively reduced the HC yield. At a constant residence time of 2 h, the yield decreased from approximately 63.6 % (HC160–2) to 53.6 % (HC200–2). Similarly, increasing the residence time at a constant temperature consistently reduced the yield. For instance, at 180 °C, the yield decreased from 59.8 % (HC180–2) to 53.2 % (HC180–4) and further to 47.4 % (HC180–6). The highest HC yield of approximately 63.6 % was obtained under the mildest conditions (HC160–2). This trend could be attributed to the gradual breakdown of lignocellulosic components into water-soluble and gaseous compounds under more severe hydrothermal conditions, resulting from hydrolysis, dehydration, decarboxylation, and condenzation reactions [47].

Fig. 1b shows the MB removal efficiency achieved by different HC samples. Among all tested conditions, HC prepared at 180 °C for 2 h (HC-180–2) exhibited the superior adsorption performance for MB removal. The sample removed up to 63.7 % of 50 mg/L MB within 30 min, yielding the maximum q at 31.9 mg/g. The observed temperature-dependent performance may have been attributed to the balance between surface and functional group development. At lower temperatures or shorter residence times, the development of surface functional groups and specific surface area necessary for effective MB adsorption was insufficient. The hydrolysis reaction is partial, and the biomass maintains more of its original structure with fewer pores [48]. Conversely, higher hydrothermal temperatures or extended residence times could lead to the degradation of functional groups that contribute to dye adsorption. Elevated temperatures contributed to the loss of hydroxyl and carboxyl groups, which may play crucial roles in MB adsorption mechanisms [48]. Based on these results, HC-180–2 was selected as the optimal sample for subsequent adsorption experiments and characterization analyses.

The influence of HC dosage on MB removal was investigated, and the results are illustrated in Fig. 1b Increasing HC doses increased overall MB removal, with q reaching its maximum at 1 g/L. This observation indicated that although higher dosages provided more available binding sites, optimal utilization occurred at a moderate dosage. Consequently, 1 g/L was established as the optimal HC dose for all subsequent experiments.

The results of kinetic experiments are shown in Fig. 2. HC-180–2 demonstrated an initial MB removal efficiency of 42.4 % within the first minute of contact (Fig. 2a). The adsorbent reached maximum adsorption performance at 150 min, achieving 79.3 % MB removal efficiency with a corresponding q value of 39.6 mg/g (Fig. 2a). Beyond this contact time, no significant improvement in removal efficiency was observed, indicating the establishment of adsorption equilibrium.

To clarify the underlying adsorption mechanism, both linearized and non-linearized kinetic models were applied to the experimental data (Figs. 2b and 2d). The essential values derived from the kinetic models are presented in Table 1. The pseudo-second-order kinetic models provided superior correlation with the experimental results. The model assumes that the rate-limiting step depends on the changes in concentration of both adsorbate (MB) and adsorbent (HC), and that the adsorption involves chemical interactions [49]. The results suggest that chemisorption processes, rather than physisorption, predominantly govern the adsorption of MB onto HC-180–2. The pseudo-second-order models predicted the q_e values to be 30.5 (linearized) and 34.9 mg/g (non-linearized), which were lower than the experimental q (39.6 mg/g).

The adsorption performance of HC-180–2 was evaluated under varying initial MB concentrations and temperature conditions, and the results are shown in Fig. 3a. The temperature-dependent behavior indicated that higher temperatures enhanced the MB uptake by HC-180–2. The maximum q at 25 °C was 51.6 mg/g, when a 300 mg/L initial MB concentration was used. The value increased to 59.2 mg/g at 65 °C. The positive temperature effect supported the chemisorption

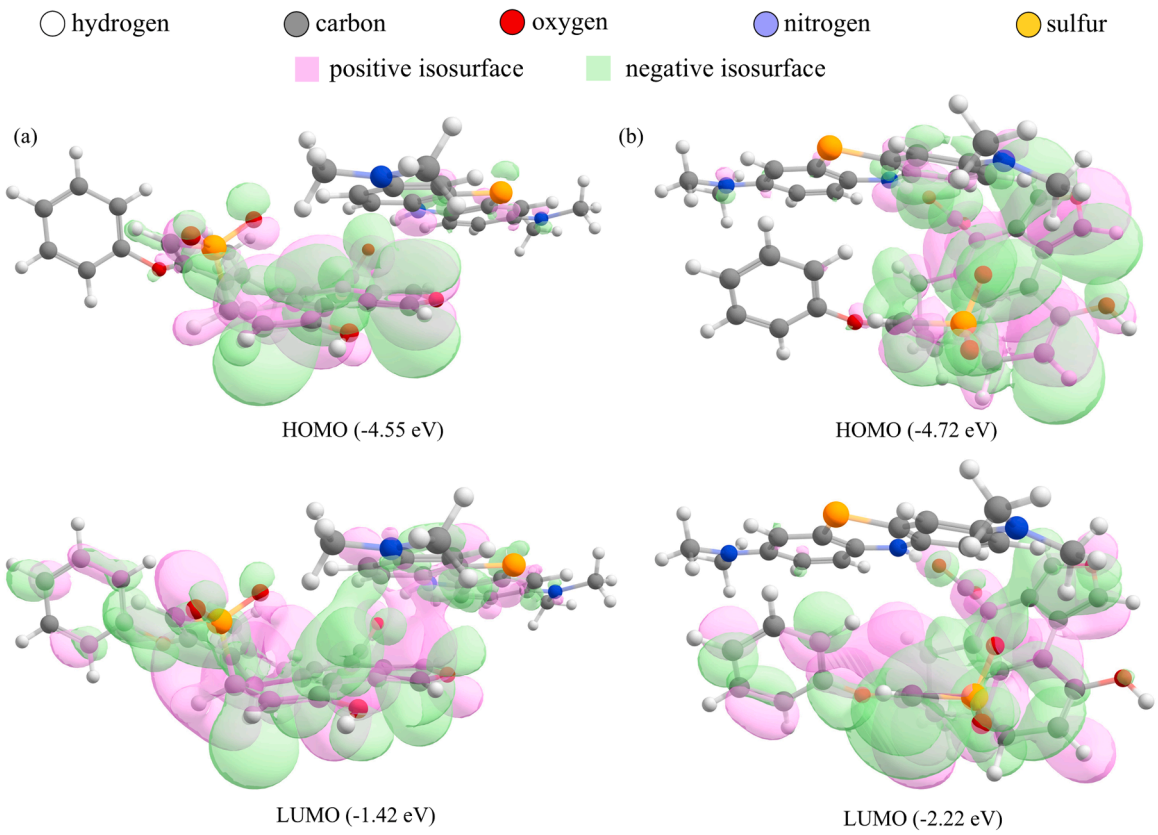

Fig. 6. Quantum theory of atoms in molecules (QTAIM) analysis with nuclear critical point (3,−3), bond critical point (3,−1), ring critical point (3,+1), cage critical point (3,+3), and bond paths: (a) HC-MB conformation 1, (b) HC-MB conformation 2.

mechanism previously identified through kinetic studies, as chemical adsorption processes typically require thermal energy to overcome the energy barriers associated with bond formation between the adsorbate and the adsorbent. This is fundamentally different from physisorption processes, where increased temperature typically reduces adsorption efficiency due to enhanced molecular kinetic energy that weakens the physical interactions [50].

Adsorption isotherms were constructed using data obtained at room temperature, which were subsequently fitted to both the Langmuir (Fig. 3b) and the Freundlich isotherm models (Fig. 3c). The derived fitting parameters for both isotherm models are presented in Table 2. The Langmuir isotherm model exhibited superior correlation with experimental data for MB adsorption onto HC-180–2 relative to the Freundlich model. The q_{max} value predicted by the Langmuir isotherm was 54.3 mg/g, slightly higher than the experimental q (51.6 mg/g). The applicability of the Langmuir isotherm indicated that the adsorption process occurred on energetically uniform sites with equal binding energies, while lateral interactions between adsorbed MB were regarded as negligible [51]. The model additionally assumed monolayer coverage, where each adsorption site bound a single MB [51].

The D-R model fitting (Fig. 3d) yielded a q_{max} of 61.9 mg/g with a high correlation coefficient ($R^2 = 0.971$). The value was in agreement with those of experimental data (51.6 mg/g) and the Langmuir-predicted value (54.3 mg/g). $E_{D\text{-}R}$ was calculated to be 5.66 kJ/mol, which falls below the threshold of 8 kJ/mol often associated with physical adsorption. However, it is important to note that the $E_{D\text{-}R}$ had limitations when applied to solid-water interface systems and cannot be reliably used to distinguish between physisorption and chemisorption in aqueous solutions [52]. Therefore, the determination of the adsorption mechanism should be based primarily on thermodynamic parameters.

The thermodynamic parameters are listed in Table 3. The fittings of the Langmuir isotherm model for all temperature conditions are presented in the supplementary material (Fig. S2). The ΔH value was 48.5 kJ/mol for the adsorption of MB by HC-180–2, indicating an endothermic enthalpy. Adsorption at the solid-liquid interface represents a competitive process involving the desorption of pre-existing water molecules from active sites and the simultaneous adsorption of solute species [53]. The endothermic nature usually occurs when adsorbate molecules must displace multiple water molecules during adsorption [53]. The positive ΔS value of 0.307 indicated an increase in randomness at the HC-MB interface. The combination of a positive ΔH and ΔS yielded negative ΔG values across all temperatures, indicating spontaneous adsorption. Typically, physisorption processes are characterized by ΔG values ranging from −20 to 0 kJ/mol, whereas chemisorption involves significantly more negative values between −80 and −400 kJ/mol [54]. This means the ΔG values in this study, ranging from −43.0 to −55.3 kJ/mol, suggested an intermediate adsorption mechanism. However, given that the kinetic data fit best with the pseudo-second-order model, the adsorption process was predominantly chemisorption.

The reusability of HC-180–2 was evaluated over 6 adsorption-regeneration cycles, as shown in Fig. 3f. The removal efficiency progressively declined with each regeneration cycle. After the first regeneration cycle, the efficiency decreased to approximately 57.7 %. The decline continued through subsequent cycles, with the removal efficiency dropping to approximately 3.06 % for cycle 6.

3.2. Hydrochar characterization

The surface and porous properties of durian peels and HC-180–2 are shown in Table 4. The BET surface area of the HC-180–2 increased from 3.04 m^2/g to 6.36 m^2/g, representing a twofold enhancement compared to the raw biomass. This modest surface area transformation contrasts with previous studies on activated carbon, which have reported surface

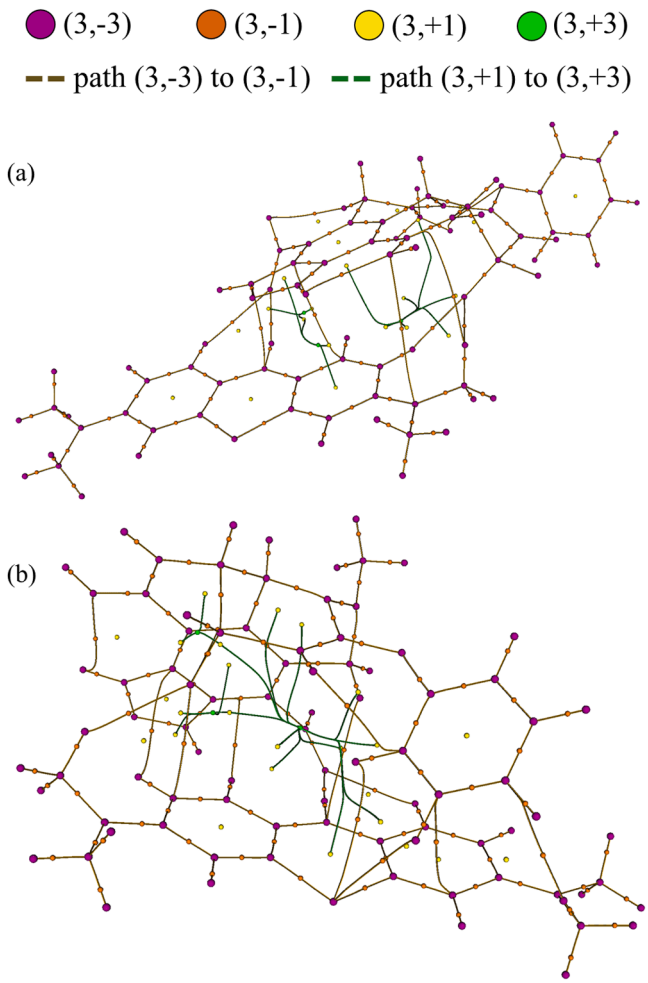

Fig. 7. Molecular orbital, highest occupied molecular orbital (HOMO) and lowest unoccupied molecular orbital (LUMO): (a) MB-HC conformation 1, (b) MB-HC conformation 2.

areas of 34.4 m^2/g [55] and 661.3 m^2/g [56]. The BJH average pore diameter also expanded from 16 nm in the biomass to 29.9 nm in HC-180–2. This structural modification was reminiscent of a previous study, which demonstrated that mesoporous structures with pore diameters around 3.03 nm can effectively capture methylene blue molecules (1.43 nm in size) [55]. These minute increases in HC surface area and pore volume further support the chemisorption mechanism of the adsorption system. Carbon-based adsorbents employing physisorption for MB adsorption can achieve BET surface areas up to 2000 m^2/g [57]. However, the pore structure and surface chemistry are more critical than absolute surface area for dye adsorption [56]. Chemisorption primarily depends on surface chemical functionality rather than a high surface area, as moderate BET surface areas are sufficient when the surface chemistry enables the formation of strong chemical bonds [58].

EDX analysis results are tabulated in Table 5. The analysis shows that durian peels contain magnesium (Mg, 0.33 %) and potassium (K, 1.3 %). These minerals are naturally found in the biomass [59]. Following hydrothermal treatment, Mg and K were removed while carbon (C), oxygen (O), and sulfur (S) were retained. An ultimate analysis from previous research revealed that durian peels can contain up to 0.1 wt % amino acids [60]. Specifically, cysteine and methionine might be present as they are key sulfur-containing protein components found in durian and its peels [61]. The increase in sulfur after adsorption was due to the uptake of MB.

The SEM images, available in the supplementary material (Fig. S3), revealed few visible changes in the surface topology of the samples. The durian peels (Fig. S3a) exhibit a fibrous, layered structure with irregular surfaces characteristic of lignocellulosic biomass. HC-180–2 (Fig. S3b) morphology shows that the fibrous structure is largely preserved. This minimal morphological alteration suggests that the HTC conditions employed (180 °C, 2 h) are relatively mild and do not cause extensive physical alteration of the biomass matrix. After MB adsorption (Fig. S4c), the HC-180–2 surface morphology remains similar to that before adsorption.

FTIR analysis in Fig. 4a reveals significant structural transformations after the HTC of durian peels. The raw biomass displayed characteristic peaks at 3300 cm^{-1} (OH stretching) and 1740 cm^{-1} ($C = O$ aldehyde), with the latter disappearing after HC formation. Hydrothermal treatment enhanced several functional groups, including OH stretching (3300 cm^{-1}), aliphatic C—H stretching (2920 cm^{-1}), and C—H bending vibrations (1370 cm^{-1}). New peaks emerged in the HC sample, indicating increased aromatization with $C = C$ stretching around 1600–1650 cm^{-1} and strong aromatic C—C stretching at 1510 cm^{-1}. The formation of sulfone groups was evidenced by $S = O$ stretching at 1160 cm^{-1}, while ester functionalities appeared at 1165 cm^{-1} (C—O stretching). The prominent anhydride peak at 1025 cm^{-1} (CO—O-CO stretching) and alkene bending at 900 cm^{-1} further confirmed structural modifications during carbonization. Following MB adsorption, additional peaks at 1600 cm^{-1} (CH=N) and 881 cm^{-1} (C—H bending) confirmed dye uptake, while the shift in aromatic C—C peaks suggested possible interactions between the HC and MB. The Raman shifts in Fig. 4b corroborate the FTIR functional group analysis. The G-band (1580 – 1600 cm^{-1}) corresponds to ordered graphitic carbon with in-plane sp^2 vibrations, while

Table 7
Comparison of MB adsorption capacity and operating conditions for HC derived from various biomass feedstocks under different hydrothermal treatment and modification conditions (HC in all studies were made under autogenous pressure).

biomass	hydrothermal treatment		adsorption of MB				Ref.
	condition	modification	maximum q (mg/g)	equilibrium time (min)	C_0 (mg/L)	adsorption temperature (°C)	
durian peels	200 °C, 4 h	no modification	51.6	150	300	room temperature	this study
bamboo with PVC	230 °C, 24 h	NaOH	259	360	400	25.0	[28]
cotton straw	200 °C, 12 h,	iron citrate, pyrolysis at 800 °C	660	200	n/a	n/a	[38]
corncobs	180 °C, 6 h	KOH and pyrolysis at 800 °C	490	300	500	30.0	[63]
wheat straw	220 °C, 12 h	KOH	24.5	120	40.0	25.0	[64]
grape pomace	220 °C, 1 h	magnesium, NaOH and pyrolysis at 300 °C	290	500	600	25.0	[65]
sunflower stalks	220 °C, 2 h	no modification	24.1	240	50.0	room temperature	[66]

n/a – not available.
q – adsorption capacity.
C_0 – initial MB concentration.

the D-band (1300 – 1360 cm^{-1}) signifies structural disorder and defects through out-of-plane vibrations in fused aromatic rings and amorphous carbon regions. Based on the FTIR and Raman spectral data, a proposed HC structure is constructed and illustrated in Fig. 4c.

3.3. Computational study and mechanism of methylene blue adsorption

The optimized structures of MB and HC are shown in Figs. 5a and 5b, respectively. The DFT calculation yielded two optimized HC-MB conformations, which are displayed in Figs. 5c and 5d The molecular interactions between HC and MB are tabulated in Table 6, which details all bond types and their distances between the functional groups involved in the two conformations. Conformation 1 ($E = -149.95$ Eh) was the more thermodynamically favourable arrangement, featuring a typical hydrogen bond between the carboxylic acid (H-donor) of HC and the amine (H-acceptor) of MB at 1.81 Å. The carbon-hydrogen bond involving the sulfone group (H-acceptor) of HC and the methyl group (H-donor) of MB had a distance of 2.64 Å. This conformation also exhibited π-π stacking interactions between benzene derivatives at three distances (4.11, 3.69, and 3.37 Å), indicating multiple aromatic interactions, along with a π-sulfur stacked interaction at 5.81 Å between the sulfone group of HC and the aromatic system of MB. Conversely, conformation 2 ($E = -149.89$ Eh), while slightly less stable, showed a stronger hydrogen bond at 1.74 Å and a more compact carbon-hydrogen interaction at 2.46 Å. However, it exhibited weaker π-π stacking at longer distances (4.63 and 5.13 Å). The conformation also featured π-sulfur interactions involving both the sulfone (4.42 Å) and the thioether groups (4.58 Å). The energy difference of 0.06 Eh between the conformations suggests that both binding modes are energetically feasible, involving hydrogen bonding, aromatic stacking, and sulfur-mediated interactions.

The QTAIM analysis in Fig. 6 also provides evidence for the chemisorption of MB on HC by revealing the formation of chemical bonds. The presence of the bond critical points (3,−1) demonstrated covalent bond formation, while the bond paths trace the electron-density pathways connecting the interacting atoms between MB and HC in both conformations. The nuclear critical points (3,−3), ring critical points (3,+1), and cage critical points (3,+3) mapped the topological electron density, confirming that the interaction went beyond physisorption to involve chemical bonding with shared electron density between the MB and functional groups of HC. Separate critical points (3,−1)

Based on the molecular orbital analysis shown in Fig. 7, the chemisorption of MB onto HC involves significant electronic interactions between the two systems. In conformation 1 (Fig. 7a), the HOMO-LUMO gap is 3.13 eV (HOMO at −4.55 eV, LUMO at −1.42 eV), while in conformation 2 (Fig. 7b), the gap is smaller at 2.50 eV (HOMO at −4.72 eV, LUMO at −2.22 eV). The orbital isosurface visualizations reveal substantial orbital overlap between the MB dye molecule and the biochar surface, with both positive (pink) and negative (green) isosurfaces indicating strong electronic coupling. The presence of heteroatoms (nitrogen, oxygen, and sulfur) in both the HC and MB structures facilitates charge-transfer interactions, as evidenced by the delocalized electron density extending across the interface. The smaller HOMO-LUMO gap in conformation 2 suggests stronger electronic interactions and a higher binding affinity. The smaller HOMO-LUMO gap in conformation 2, combined with its higher total energy (Eh = −149.89 Eh compared to −149.95 Eh for conformation 1), suggests that while conformation 1 is thermodynamically more stable, conformation 2 exhibits enhanced electronic reactivity due to its reduced energy barrier for electron transitions. This orbital analysis confirms that the HC-MB interaction involves significant electronic coupling and charge redistribution rather than simple physical adsorption. A previous study also demonstrated chemisorptive interactions between nanocages and cisplatin in the aqueous phase, with energy gaps ranging from 0.885 to 3.15 eV [67]. Similarly, a DFT study of chemical adsorption for different gas molecules (CO, N_2, NO, etc.) on graphene nanoflakes yielded energy gaps ranging from 1.81 to 4.13 eV [68].

3.4. Comparison to other studies on methylene blue adsorption on hydrochar

The HTC of durian peels in this study yielded HC with a moderate MB adsorption capacity (51.6 mg/g) when compared to HC samples from previous studies tabulated in Table 7. This adsorption capacity was achieved within a reasonable equilibrium time of 150 min at room temperature without any chemical modification. While this adsorption capacity was lower compared to chemically modified HC such as NaOH-treated bamboo with PVC (259 mg/g), iron citrate and pyrolysis-treated cotton straw (660 mg/g), and KOH-treated corncobs (490 mg/g), the unmodified durian peels HC demonstrated several advantages including environmental sustainability due to the absence of harsh chemical treatments, ambient temperature operation eliminating additional energy requirements, and a relatively fast equilibrium time compared to bamboo (360 min) and cotton straw (200 min). The adsorption performance was comparable to that of unmodified sunflower stalks (24.1 mg/g). The operational simplicity and environmental compatibility of durian peels HC positioned it as a promising eco-friendly adsorbent for MB removal applications, where moderate adsorption capacity with sustainable processing conditions was preferred over maximum adsorption performance requiring intensive chemical modifications.

4. Conclusions

Durian peels-derived HC produced through HTC at 180 °C for 2 h demonstrated effective MB removal capabilities. It yielded a q value of 51.6 mg/g at room temperature, with an equilibrium time of 150 min. The q value increased to 59.2 mg/g when the adsorption condition was elevated to 65 °C. The research revealed that MB adsorption onto durian peel HC followed a chemisorption mechanism, as confirmed by both linear and non-linear pseudo-second-order kinetics and thermodynamic studies. The BET surface area of HC-180–2 increased minimally after hydrothermal treatment, supporting a chemisorption mechanism that depends on surface chemical functionality rather than high surface area. EDX analysis revealed that the hydrothermal treatment removed minerals while retaining C, O, and S, the last of which originated from amino acids naturally present in the durian peels. FTIR and Raman analyses confirmed structural transformations, including enhanced aromatization, formation of sulfone and ester groups, while post-adsorption FTIR spectra verified MB uptake by the HC. Computational chemistry analysis using DFT identified hydrogen bonding between the carboxylic acid groups of HC and the amine groups of MB, complemented by π-π stacking and π-sulfur interactions. The HOMO-LUMO gaps of 2.5 and 3.13 eV for the two most stable HC-MB conformations further validated the chemisorption nature. The QTAIM analysis confirmed the formation of chemical bonds through electron-density pathways. The adsorption capacity was deemed moderate compared with that of chemically modified adsorbents. Future research directions should focus on optimizing hydrothermal conditions to enhance surface area and functional group development and performing comprehensive life cycle assessments to quantify the environmental benefits compared to conventional treatment methods. All in all, the minimally modified durian peels HC offers a significant advantage in terms of sustainability, energy efficiency, and processing simplicity as an MB removal agent.

Funding information

This work is supported by the Strategic Research Fund (Starter, Contract no MU-SRF-ST-01A/67) granted by Mahidol University.

CRediT authorship contribution statement

Piangjai Peerakiatkhajohn: Writing – original draft, Project

administration, Methodology, Formal analysis. **Praewa Wongburi:** Writing – review & editing, Data curation. **Kamonwat Nakason:** Writing – review & editing, Validation. **Bunyarit Panyapinyopol:** Writing – review & editing, Validation. **Khanin Nueangnoraj:** Resources, Investigation. **Phongphot Sakulaue:** Investigation, Data curation. **Davide Poggio:** Writing – review & editing, Validation. **William Nimmo:** Writing – review & editing, Validation. **Jakkapon Phanthuwongpakdee:** Writing – original draft, Supervision, Software, Project administration, Methodology, Funding acquisition, Conceptualization.

Declaration of competing interest

The authors declare that they have no known competing financial interests or personal relationships that could have appeared to influence the work reported in this paper.

Acknowledgements

This research project is supported by Mahidol University (Strategic Research Fund, 2024, contract no MU-SRF-ST-01A/67). The authors would also like to thank Jinnaphat Bamrungna, Parinchana Samerwai, and Pitchawanda Sripalin for their support in laboratory work.

Supplementary materials

Supplementary material associated with this article can be found, in the online version, at doi:10.1016/j.ceja.2025.101011.

Data availability

Data will be made available on request.

References

[1] I. Khan, K. Saeed, I. Zekker, B. Zhang, A.H. Hendi, A. Ahmad, et al., Review on Methylene blue: its properties, uses, toxicity and photodegradation, Water (Basel) 14 (2022) 242, https://doi.org/10.3390/w14020242.
[2] T. Islam, Repon MdR, T. Islam, Z. Sarwar, M.M. Rahman, Impact of textile dyes on health and ecosystem: a review of structure, causes, and potential solutions, Environ. Sci. Pollut. Res. 30 (2022) 9207–9242, https://doi.org/10.1007/s11356-022-24398-3.
[3] S.S. Auerbach, D.W. Bristol, J.C. Peckham, G.S. Travlos, C.D. Hébert, R.S. Chhabra, Toxicity and carcinogenicity studies of methylene blue trihydrate in F344N rats and B6C3F1 mice, Food Chem. Toxicol. 48 (2010) 169–177, https://doi.org/10.1016/j.fct.2009.09.034.
[4] P.O. Oladoye, T.O. Ajiboye, E.O. Omotola, O.J. Oyewola, Methylene blue dye: toxicity and potential elimination technology from wastewater, Results Eng. 16 (2022) 100678, https://doi.org/10.1016/j.rineng.2022.100678.
[5] A.K. Raj, Adsorption of methylene blue dye from textile industry effluent using activated carbon synthesized from various plant-based precursors, Orient. J. Chem. 41 (2025), https://doi.org/10.13005/ojc/410236.
[6] N. Renugadevi, R. Sangeetha, P. Lalitha, Kinetics of the adsorption of methylene blue from an industrial dyeing effluent onto activated carbon prepared from the fruits of *Mimusops Elengi*, Arch Appl Sci Res 3 (2011) 492–498.
[7] Q.V. Vo, L.T.T. Thao, T.D. Manh, Bay M Van, B.-T. Truong-Le, N.T. Hoa, et al., Reaction of methylene blue with OH radicals in the aqueous environment: mechanism, kinetics, products and risk assessment, RSC Adv 14 (2024) 27265–27273, https://doi.org/10.1039/D4RA05437G.
[8] O.A. Urucu, B. Garosi, R.A. Musah, Efficient phytoremediation of methyl red and methylene blue dyes from aqueous solutions by *Juncus effusus*, ACS Omega 10 (2025) 1943–1953, https://doi.org/10.1021/acsomega.4c07468.
[9] A.H. Hashem, E. Saied, M.S. Hasanin, Green and ecofriendly bio-removal of methylene blue dye from aqueous solution using biologically activated banana peel waste, Sustain Chem Pharm 18 (2020) 100333, https://doi.org/10.1016/j.scp.2020.100333.
[10] R. Abdullah, A.A. Jalil, M. Asmadi, N.S. Hassan, M.B. Bahari, M. Alhassan, et al., Recent advances in zinc oxide-based photoanodes for photoelectrochemical water splitting, Int J Hydrog. Energy 107 (2025) 183–207, https://doi.org/10.1016/j.ijhydene.2024.05.461.
[11] W. Zhu, Z. Wu, S. Zhao, F. Lv, Y. Zhang, S. Guo, Selective adsorption and separation of methylene blue from wastewater by self-standing polyvinylpyrrolidone and SiO2 electrospun membranes, Chem Eng Sci 280 (2023) 119009, https://doi.org/10.1016/j.ces.2023.119009.
[12] J. Cheng, C. Zhan, J. Wu, Z. Cui, J. Si, Q. Wang, et al., Highly efficient removal of methylene blue dye from an aqueous solution using cellulose acetate nanofibrous membranes modified by polydopamine, ACS Omega 5 (2020) 5389–5400, https://doi.org/10.1021/acsomega.9b04425.
[13] N. Noreen, M. Kazmi, N. Feroze, F. Javed, H.G. Qutab, H.M.S. Munir, Treatment of methylene blue in aqueous solution by electrocoagulation/micro-crystalline cellulosic adsorption combined process, Desalin. Water Treat 203 (2020) 379–387, https://doi.org/10.5004/dwt.2020.26213.
[14] S. Ihaddaden, D. Aberkane, A. Boukerroui, D. Robert, Removal of methylene blue (basic dye) by coagulation-flocculation with biomaterials (bentonite and Opuntia ficus indica), J. Water Process Eng. 49 (2022) 102952, https://doi.org/10.1016/j.jwpe.2022.102952.
[15] S. Mishra, N. Chakinala, A.G. Chakinala, P.K. Surolia, Photocatalytic degradation of methylene blue using monometallic and bimetallic Bi-Fe doped TiO2, Catal Commun 171 (2022) 106518, https://doi.org/10.1016/j.catcom.2022.106518.
[16] D. Atta, H.A. Wahab, M.A. Ibrahim, I.K. Battisha, Photocatalytic degradation of methylene blue dye by ZnO nanoparticle thin films, using sol–gel technique and UV laser irradiation, Sci Rep 14 (2024) 26961, https://doi.org/10.1038/s41598-024-76938-1.
[17] J. Fito, M. Abewaa, A. Mengistu, K. Angassa, A.D. Ambaye, W. Moyo, et al., Adsorption of methylene blue from textile industrial wastewater using activated carbon developed from Rumex abyssinicus plant, Sci Rep 13 (2023) 5427, https://doi.org/10.1038/s41598-023-32341-w.
[18] D. Dimbo, M. Abewaa, E. Adino, A. Mengistu, T. Takele, A. Oro, et al., Methylene blue adsorption from aqueous solution using activated carbon of spathodea campanulata, Results Eng. 21 (2024) 101910, https://doi.org/10.1016/j.rineng.2024.101910.
[19] Al-Asadi ST, Z.H. Mussa, Al-Qaim FF, H. Kamyab, Al-Saedi HFS, I.F. Deyab, et al., A comprehensive review of methylene blue dye adsorption on activated carbon from edible fruit seeds: a case study on kinetics and adsorption models, Carbon Trends 20 (2025) 100507, https://doi.org/10.1016/j.cartre.2025.100507.
[20] B. Tewabe Gebeyehu, D. Manaye Kabtamu, T. Alehegne Tasew, Efficient removal of methylene blue dye from aqueous solution using a new biosorbent derived from Ensete ventricosum (Enset), Bull Chem Soc Ethiop 38 (2023) 69–84, https://doi.org/10.4314/bcse.v38i1.6.
[21] M.B. Goudjil, H. Dali, S. Zighmi, Z. Mahcene, S.E. Bencheikh, Photocatalytic degradation of methylene blue dye with biosynthesized hematite α-Fe2O3 nanoparticles under UV-irradiation, Desalin. Water Treat 317 (2024) 100079, https://doi.org/10.1016/j.dwt.2024.100079.
[22] Z. Kalaycıoğlu, B. Özuğur Uysal, Ö. Pekcan, F.B Erim, Efficient photocatalytic degradation of methylene blue dye from aqueous solution with cerium oxide nanoparticles and graphene oxide-doped polyacrylamide, ACS Omega 8 (2023) 13004–13015, https://doi.org/10.1021/acsomega.3c00198.
[23] S. Nengsih, S. Nur Abdulmadjid, M. Mursal, Z. Jalil, Photocatalytic performance of Fe3O4-TiO2 in the degradation of methylene blue dye: optimizing the usability of natural iron sand, Mater Sci Energy Technol 7 (2024) 374–380, https://doi.org/10.1016/j.mset.2024.06.001.
[24] M. Gęca, M. Wiśniewska, P. Nowicki, Biochars and activated carbons as adsorbents of inorganic and organic compounds from multicomponent systems – A review, Adv Colloid Interface Sci 305 (2022) 102687, https://doi.org/10.1016/j.cis.2022.102687.
[25] Q. Guo, S. Qiao, D. Zhang, Z. Zhang, F. Yu, Z. Ma, et al., A comparison of hydrothermal carbonization versus pyrolysis-activation for sludge-derived carbon materials on physiochemical properties and electrochemical performance, Biomass Bioenergy 182 (2024) 107079, https://doi.org/10.1016/j.biombioe.2024.107079.
[26] M. Elhassan, R. Abdullah, M.R.R. Kooh, Y.-F. Chou Chau, Hydrothermal liquefaction: a technological review on reactor design and operating parameters, Bioresour Technol Rep 21 (2023) 101314, https://doi.org/10.1016/j.biteb.2022.101314.
[27] S. Kousar, M. Fan, K. Javed, M. Rashid, S. Zhang, X. Hu, Hydrothermal carbonization of fruit peels of varied origin forms hydrochar of distinct capability for adsorption of methylene blue, J. Water Process Eng. 65 (2024), https://doi.org/10.1016/j.jwpe.2024.105799.
[28] H.Z. Li, Y.N. Zhang, J.Z. Guo, J.Q. Lv, W.W. Huan, B. Li, Preparation of hydrochar with high adsorption performance for methylene blue by co-hydrothermal carbonization of polyvinyl chloride and bamboo, Bioresour Technol 337 (2021), https://doi.org/10.1016/j.biortech.2021.125442.
[29] S. Semae, T. Kraiprom, R. Wamaedeesa, R. Umar, N. Hilae, A. Auseng, et al., The durian peel waste as high-quality feed on goat performance and economic worthiness, Int. J. Sci. Innov. Technol. 7 (2024).
[30] The Nation, Fruit yields up in 2025; Durian hits 1.6 million tons, Nation (2025).
[31] S. Siwina, R. Leesing, Bioconversion of durian (Durio zibethinus Murr.) peel hydrolysate into biodiesel by newly isolated oleaginous yeast Rhodotorula mucilaginosa KKUSY14, Renew Energy 163 (2021) 237–245, https://doi.org/10.1016/j.renene.2020.08.138.
[32] A.R. Fauzi, D.M.D. Puspitawati, Utilization compost of durian shell to reduce dose of N inorganic fertilizer in green cabbage (*Brassica junceae*) production, AGROTROP 7 (2017) 22–30.
[33] F. Fitriani, H. Husin, M. Marwan, F. Nasution, Z. Zuhra, T.M. Asnawi, et al., Waste peel of durian as solid catayst for biodiesel production, IOP Conf Ser Mater Sci Eng 845 (2020) 012033, https://doi.org/10.1088/1757-899X/845/1/012033.
[34] Q.T. Tran, T.H. Đo, X.L. Ha, T.T.A. Duong, M.N. Chu, V.N. Vu, et al., Experimental design, equilibrium modeling and kinetic studies on the adsorption of methylene blue by adsorbent: activated carbon from durian shell waste, Mater. (Basel) 15 (2022), https://doi.org/10.3390/ma15238566.

[35] D.B. Ninh, M.D. Vu, V.A. Hoang, D.L. Vu, C.S. Kim, I.H. Nurwahid, Activated carbon-derived from durian peels for the adsorption of methylene blue dye, J Dispers Sci Technol (2025), https://doi.org/10.1080/01932691.2025.2527267.
[36] H. Sudrajat, A. Susanti, D.K.Y. Putri, S. Hartuti, Mechanistic insights into the adsorption of methylene blue by particulate durian peel waste in water, Water Sci. Technol. 84 (2021) 1774–1792, https://doi.org/10.2166/wst.2021.361.
[37] P. Zhou, X. Li, J. Zhou, Z. Peng, L. Shen, W. Li, Insights of the adsorption mechanism of methylene blue on biochar from phytoextraction residues of Citrus aurantium L.: adsorption model and DFT calculations, J Env. Chem Eng 11 (2023), https://doi.org/10.1016/j.jece.2023.110496.
[38] L. Cheng, Y. Ji, X. Liu, Insights into interfacial interaction mechanism of dyes sorption on a novel hydrochar: experimental and DFT study, Chem Eng Sci 233 (2021), https://doi.org/10.1016/j.ces.2020.116432.
[39] A. Guediri, A. Bouguettoucha, H. Tahraoui, D. Chebli, A. Amrane, J. Zhang, Thermodynamic study and the development of a support vector machine model for predicting adsorption behavior of orange peel-derived beads in wastewater treatment, J Mol Liq 403 (2024) 124860, https://doi.org/10.1016/j.molliq.2024.124860.
[40] Q. Hu, Z. Zhang, Application of Dubinin–Radushkevich isotherm model at the solid/solution interface: a theoretical analysis, J Mol Liq 277 (2019) 646–648, https://doi.org/10.1016/j.molliq.2019.01.005.
[41] A. Bouguettoucha, D. Chebli, T. Mekhalef, A. Noui, A. Amrane, The use of a forest waste biomass, cone of Pinus brutia for the removal of an anionic azo dye Congo red from aqueous medium, Desalin. Water Treat 55 (2015) 1956–1965, https://doi.org/10.1080/19443994.2014.928235.
[42] F. Neese, F. Wennmohs, U. Becker, C. Riplinger, The ORCA quantum chemistry program package, J Chem Phys 152 (2020), https://doi.org/10.1063/5.0004608.
[43] F. Neese, The SHARK integral generation and digestion system, J Comput Chem 44 (2023) 381–396, https://doi.org/10.1002/jcc.26942.
[44] T. Lu, F. Chen, Multiwfn: a multifunctional wavefunction analyzer, J Comput Chem 33 (2012) 580–592, https://doi.org/10.1002/jcc.22885.
[45] Zhurko G.A. Chemcraft 2005.
[46] BIOVIA. Discovery Studio Visualizer 2021.
[47] C.P. Odeh, C.O. Mgbemena, B.U. Oreko, C.E. Mgbemena, Impact of processing parameters on the hydrothermal carbonisation of African Elemi Shell, J. Umm Al-Qura Univ. Eng. Archit. (2025), https://doi.org/10.1007/s43995-025-00135-y.
[48] C. Chen, W. Liang, F. Fan, C. Wang, The effect of temperature on the properties of hydrochars obtained by hydrothermal carbonization of waste *camellia oleifera* shells, ACS Omega 6 (2021) 16546–16552, https://doi.org/10.1021/acsomega.1c01787.
[49] J.C. Bullen, S. Saleesongsom, K. Gallagher, D.J. Weiss, A revised pseudo-second-order kinetic model for adsorption, sensitive to changes in adsorbate and adsorbent concentrations, Langmuir 37 (2021) 3189–3201, https://doi.org/10.1021/acs.langmuir.1c00142.
[50] J.H. Potgieter, C. Pardesi, S. Pearson, A kinetic and thermodynamic investigation into the removal of methyl orange from wastewater utilizing fly ash in different process configurations, Env. Geochem Health 43 (2021) 2539–2550, https://doi.org/10.1007/s10653-020-00567-6.
[51] R.I. Masel, Principles of Adsorption and Reaction on Solid Surfaces, John Wiley & Sons, Inc., 1996.
[52] V. Puccia, M.J. Avena, On the use of the Dubinin-Radushkevich equation to distinguish between physical and chemical adsorption at the solid-water interface, Colloid Interface Sci Commun 41 (2021) 100376, https://doi.org/10.1016/j.colcom.2021.100376.
[53] P. Saha, S. Chowdhury, Insight into adsorption thermodynamics, Thermodynamics (2011), https://doi.org/10.5772/13474.
[54] D. Chebli, A. Bouguettoucha, T. Mekhalef, S. Nacef, A. Amrane, Valorization of an agricultural waste, Stipa tenassicima fibers, by biosorption of an anionic azo dye, Congo red, Desalin. Water Treat 54 (2015) 245–254, https://doi.org/10.1080/19443994.2014.880154.
[55] A.H. Jawad, M.M. Nafi, H.F. Awang, L.D. Wilson, Z.A. ALOthman, Numerical parametric optimization with desirability functions for methylene blue dye removal by sunflower seed pericarp activated carbon, Biomass Convers Biorefin 15 (2025) 11135–11149, https://doi.org/10.1007/s13399-024-05862-1.
[56] N.A.M. Hanafi, A.S. Abdulhameed, A.H. Jawad, Z.A. ALOthman, T.A. Yousef, O. K. Al Duaij, et al., Optimized removal process and tailored adsorption mechanism of crystal violet and methylene blue dyes by activated carbon derived from mixed orange peel and watermelon rind using microwave-induced ZnCl2 activation, Biomass Convers Biorefin 14 (2024) 28415–28427, https://doi.org/10.1007/s13399-022-03646-z.
[57] E. Santoso, R. Ediati, Y. Kusumawati, H. Bahruji, D.O. Sulistiono, D. Prasetyoko, Review on recent advances of carbon based adsorbent for methylene blue removal from waste water, Mater Today Chem 16 (2020) 100233, https://doi.org/10.1016/j.mtchem.2019.100233.
[58] K. Skic, A. Adamczuk, A. Gryta, P. Boguta, T. Tóth, G. Jozefaciuk, Surface areas and adsorption energies of biochars estimated from nitrogen and water vapour adsorption isotherms, Sci Rep 14 (2024) 30362, https://doi.org/10.1038/s41598-024-81030-9.
[59] N. Prakongkep, R.J. Gilkes, W. Wiriyakitnateekul, Agronomic benefits of durian shell biochar, J. Met. Mater. Miner. 24 (2014) 7–11.
[60] T.C. Chandra, M.M. Mirna, J. Sunarso, Y. Sudaryanto, S. Ismadji, Activated carbon from durian shell: preparation and characterization, J Taiwan Inst Chem Eng 40 (2009) 457–462, https://doi.org/10.1016/j.jtice.2008.10.002.
[61] L. Sangpong, G. Khaksar, P. Pinsorn, A. Oikawa, R. Sasaki, A. Erban, et al., Assessing dynamic changes of taste-related primary metabolism during ripening of durian pulp using metabolomic and transcriptomic analyses, Front Plant Sci 12 (2021), https://doi.org/10.3389/fpls.2021.687799.
[62] A.B. Brown, B.J. McKeogh, G.A. Tompsett, R. Lewis, N.A. Deskins, M.T. Timko, Structural analysis of hydrothermal char and its models by density functional theory simulation of vibrational spectroscopy, Carbon N Y 125 (2017) 614–629, https://doi.org/10.1016/j.carbon.2017.09.051.
[63] T. Hien Tran, A.H. Le, T.H. Pham, L.D. Duong, X.C. Nguyen, A.K. Nadda, et al., A sustainable, low-cost carbonaceous hydrochar adsorbent for methylene blue adsorption derived from corncobs, Env. Res 212 (2022) 113178, https://doi.org/10.1016/j.envres.2022.113178.
[64] S. Kohzadi, N. Marzban, K. Godini, N. Amini, A. Maleki, Effect of hydrochar modification on the adsorption of methylene blue from aqueous solution: an experimental study followed by intelligent modeling, Water (Basel) 15 (2023) 3220, https://doi.org/10.3390/w15183220.
[65] J. Petrović, M. Ercegović, M. Simić, D. Kalderis, M. Koprivica, J. Milojković, et al., Novel Mg-doped pyro-hydrochars as methylene blue adsorbents: adsorption behavior and mechanism, J Mol Liq 376 (2023) 121424, https://doi.org/10.1016/j.molliq.2023.121424.
[66] R. Saini, M. Pandey, R.K. Mishra, P. Kumar, Adsorption potential of hydrochar derived from hydrothermal carbonization of waste biomass towards the removal of methylene blue dye from wastewater, Biomass Convers Biorefin 15 (2025) 9229–9249, https://doi.org/10.1007/s13399-024-05743-7.
[67] Muktadir MdG, A. Alam, A.A. Piya, S.U.D. Shamim, Exploring the adsorption ability with sensitivity and reactivity of C 12 –B 6 N 6, C 12 –Al 6 N 6, and B 6 N 6 –Al 6 N 6 heteronanocages towards the cisplatin drug: a DFT, AIM, and COSMO analysis, RSC Adv 12 (2022) 29569–29584, https://doi.org/10.1039/D2RA04011E.
[68] M.H. Mohammed, F.N. Ajeel, A.M. Khudhair, Adsorption of gas molecules on graphene nanoflakes and its implication as a gas nanosensor by DFT investigations, Chin. J. Phys. 55 (2017) 1576–1582, https://doi.org/10.1016/j.cjph.2017.05.013.